MDPI

Article

Refined Assessment and Future Projections of Indian Summer Monsoon Rainfall Using CMIP6 Models

Jiahao Li [1], **Lingli Fan** [1,*], **Xuzhe Chen** [1], **Chunqiao Lin** [1], **Luchi Song** [1] and **Jianjun Xu** [2]

1   College of Ocean and Meteorology, Guangdong Ocean University, Zhanjiang 524088, China
2   Shenzhen Institute of Guangdong Ocean University, Shenzhen 518120, China
*   Correspondence: fanll@gdou.edu.cn; Tel.: +86-759-239-6055

Abstract: Analyzing and forecasting the Indian Summer Monsoon Rainfall (ISMR) is vital for South Asia's socio-economic stability. Using 35 climate models from the latest generation of the Coupled Model Intercomparison Project (CMIP6) to simulate and project ISMR, we integrated statistical methods, such as Taylor diagrams, comprehensive rating indicators, and interannual variability scores, to compare performance differences between various models and analyze influencing mechanisms. The results show that the majority of models effectively simulate the climatology of the ISMR. However, they exhibit limitations in accurately capturing its interannual variability. Importantly, we observed no significant correlation between a model's ability to simulate ISMR's general climatology and its accuracy in representing annual variability. After a comprehensive assessment, models, like BCC-ESM1, EC-Earth3-Veg, GFDL-CM4, INM-CM5-0, and SAM0-UNICON were identified as part of the prime model mean ensemble (pMME), demonstrating superior performance in spatiotemporal simulations. The pMME can accurately simulate the sea surface temperature changes in the North Indian Ocean and the atmospheric circulation characteristics of South Asia. This accuracy is pivotal for CMIP6's prime models to precisely simulate ISMR climatic variations. CMIP6 projections suggest that, by the end of the 21st century, ISMR will increase under low, medium, and high emission scenarios, with a significant rise in rainfall under the high emission scenario, especially in the western and northern parts of India. Among the pMME, the projected increase in rainfall across India is more moderate, with an estimated increase of 30%. The findings of this study suggest that selecting the best models for regional climate downscaling research will project regional climate changes more accurately. This provides valuable recommendations for model improvements in the Indian region.

Keywords: Indian summer monsoon rainfall; CMIP6; model assessment; projected rainfall trend

1. Introduction

The Indian Summer Monsoon Rainfall (ISMR), predominantly characterized by the southwest monsoon precipitation spanning June to September in the Indian domain, underpins the agricultural ecosystem, food and water security, societal welfare, and economic stability of the densely populated South Asia [1,2]. Given its paramount significance, precise analysis and prognostication of ISMR are pivotal for ensuring the region's socio-economic equilibrium.

Global Climate Models (GCMs) stand out as indispensable instruments for both retrospective simulations and prospective delineations of monsoon rainfall dynamics. As a result, the efficacy of GCMs in capturing and predicting the Indian Summer Monsoon (ISM) nuances has been a focal point of extensive scrutiny [3,4]. Notwithstanding the iterative advancements in GCMs, achieving a precise simulation of the ISM remains an intricate endeavor [3,5,6]. Contemporary research underscores that from CMIP's third to fifth iterations, a majority of models have consistently undervalued the ISM's vigor, culminating in a diminished simulated rainfall quotient over India and its vicinities [7,8]. The CMIP models exhibit poor performance in simulating the interannual variability of the South

Asian monsoon rainfall, failing to reproduce the observed interannual variations in precipitation [9,10]. This limitation highlights a critical gap in the models' ability to accurately simulate key climatic phenomena in the region. Scholars postulate that such simulation discrepancies might emanate from a confluence of determinants, like equatorial tropical sea surface temperature oscillations, intricate oceanic–atmospheric coupling dynamics, and South Asia's unique topography [5,8,11,12]. Furthermore, Woo et al., leveraging CMIP5 climate models, discerned that under RCP paradigms, both the monsoonal and extreme precipitation events in South Asia are poised for an uptick by the latter half of the 21st century [13]. Jayasankar et al., accentuated that while India's future thermal projections unequivocally signal an uptrend, the ISMR's prospective alterations manifest considerable heterogeneity across distinct CMIP5 models [14].

The Coupled Model Intercomparison Project's sixth phase (CMIP6) unveiled an array of refined GCMs, rectifying numerous limitations observed in CMIP5, such as the overestimation of both annual and seasonal precipitation totals. Moreover, the models have benefited from enhanced physical algorithms. These models now integrate the "Shared Socioeconomic Pathways" (SSPs), which prioritize a cohesive alignment between future radiative forcing scenarios and socioeconomic narratives, diverging from the traditional RCP scenario experiments [3,15]. These methodological advancements furnish critical data, bolstering the evaluation of CMIP6's aptitude in simulating current climate dynamics and forecasting future climatic trajectories [16]. A study spearheaded by He et al. scrutinized the simulation prowess of models spanning CMIP3 to CMIP6 concerning South Asian monsoon precipitation. Their findings underscored that a significant portion of CMIP6 models demonstrated reduced biases in capturing the intrinsic characteristics of ISMR and the sea surface temperature anomalies in the Northern Indian Ocean (NIO) compared to their predecessors [17,18]. Intriguingly, the multi-model ensemble average (MME) consistently outshined the Atmospheric Model Intercomparison Project (AMIP) in simulation fidelity. Drawing from diverse SSP emission scenarios within CMIP6, the MME anticipates a substantial augmentation in South Asian precipitation (10–36%), underscored by pronounced spatial heterogeneity. This underscores a palpable uncertainty regarding regional future precipitation probabilities, with CMIP6's inherent projection ambiguity marginally surpassing that of CMIP5 [19]. Historically, research endeavors have seldom delved into the intricate performance dynamics of individual models encapsulated within CMIP6. Pertinent questions arise: How stark are the disparities between the prime and nonperforming model ensembles in historical simulations? How might these variances be reflected in future projections? And, juxtaposed against CMIP5, what catalyzes the discernible enhancements in simulation biases within CMIP6? These pivotal inquiries form the crux of this manuscript. A meticulous exploration of CMIP6's prime models, particularly concerning the rectification of precipitation biases and their projected alterations, promises to mitigate model evaluation ambiguities and fortify our conviction in climate prognostications.

2. Data and Methods

2.1. Data

This study leverages monthly average simulation data sourced from 35 models within the purview of CMIP6's historical simulations. Notably, out of these, 22 models furnish data spanning three prospective emission scenarios: SSP1-2.6, SSP2-4.5, and SSP5-8.5. For more detailed information on modes, please refer to the website (https://esgf-index1.ceda.ac.uk/search/cmip6-ceda/) (accessed on 15 September 2023). The span from 1979 to 2014 serves as the historical reference period, while projections from 2015 to 2100 delineate the future analysis timeframe. Given the disparities in data resolutions, we employed a bilinear interpolation technique to standardize all model data onto a consistent 2.5° × 2.5° grid for meticulous analysis.

For a juxtaposition against the model data, the observational datasets incorporated the following: (1) Monthly global precipitation metrics courtesy of the Global Precipitation

Climatology Project (GPCP V2.3), which offers data with a spatial resolution of $2.5° \times 2.5°$ latitude/longitude; (2) The Extended Reconstructed Sea Surface Temperature (ERSST V3b) dataset, a monthly sea surface temperature log, curated by the National Oceanic and Atmospheric Administration; (3) Reanalysis datasets encapsulating zonal wind, meridional wind, geopotential height, and sea-level pressure, all furnished by the fifth-generation European Centre for Medium-Range Weather Forecasts (ECMWF). These datasets are pivotal in gauging the model's proficiency in ISMR simulations and pinpointing any inherent biases.

2.2. Methods

All-India Rainfall Index (AIRI): Following Liu's [20] definition of the monsoon region, the Indian monsoon rainfall area is delineated as (10° N~30° N, 65° E~95° E). Based on the boundaries of India, the spatially averaged total monsoon rainfall for the year is calculated. Different latitudinal regions are assigned latitudinal weights to reflect the contribution of precipitation at various latitudes.

Indian Monsoon Index (IMI): As defined by Ruiqing Li [21], IMI = U_{850}(40~80° E, 5~15° N) − U_{850}(60~90° E, 20~30° N), which describes the wind field direction caused by the Indian monsoon trough, indicating the southwest monsoon. It has a strong correlation with AIRI.

Taylor Diagram: Used to assess the similarity of climate or hydrological models to observational data on a spatial grid. It collectively displays three metrics: the Pearson correlation coefficient (PCC), the ratio of standard deviations (SDR), and the root mean square error (RMSE), offering a straightforward evaluation of model performance [22].

Comprehensive Rating Indicator: Integrates multiple evaluation metrics to quantify the simulation performance level of a model, assessing its simulation merits and shortcomings [23]. It is calculated as follows:

$$M_R = 1 - \frac{1}{n \times m}\sum_{i=1}^{n} r_i \tag{1}$$

where n represents the number of indicators used for evaluation; m is the number of models participating in the evaluation; r_i represents the ranking of a particular statistical indicator simulated by the CMIP6 model. The model with the best simulation performance has an r_i value of 1, while the model with the weakest simulation performance has an r_i value of m. Ultimately, the closer the comprehensive indicator M_R is to 1, the more exceptional the model's simulation performance.

Interannual Variability Score (IVS): Used to assess a model's simulation performance of ISMR's interannual variability [9,24]. It is calculated as follows:

$$\text{IVS} = \left(\frac{STD_m}{STD_o} - \frac{STD_o}{STD_m}\right)^2 \tag{2}$$

where STD_m and STD_o denote the interannual standard deviations of the model and observation, respectively. IVS serves as a variability metric, quantifying the congruence of interannual fluctuations between the model and observation. A diminished IVS value signifies enhanced alignment between the simulated and observed data.

3. Results

3.1. Assessment of CMIP6's Historical Simulation Capabilities for the ISMR

3.1.1. Evaluation for Spatial Variation

A hallmark of the ISM is the pronounced cross-equatorial airflow, stretching from the Somali coast to the center of the Indian Ocean, coupled with heavy rainfall blanketing India and its neighboring regions [5]. Observational data (Figure 1a) underscore the pivotal role of this cross-equatorial southwest airflow, with rainfall in India decreasing from south to north. The eastern swath of India, along with the Western Ghats, is particularly drenched.

Turning to the model simulations (Figure 1b), it's evident that CMIP6 models adeptly encapsulate the quintessence of ISMR. However, they exhibit a propensity to downplay the vigor when portraying the low-altitude airflow over the northern expanses of the Indian Ocean and the Bay of Bengal, and similarly, the rainfall intensity in central and eastern India. This observation resonates with the documented attenuation of the ISM in prior coupled model investigations [4,5,7]. It is worth spotlighting the pronounced positive rainfall biases evident in the Indian Ocean and the Western Ghats, as depicted in Figure 1c. Indeed, these surging rainfall anomalies skirting the ocean's periphery can be squarely attributed to the model's muted representation of the ISM [17].
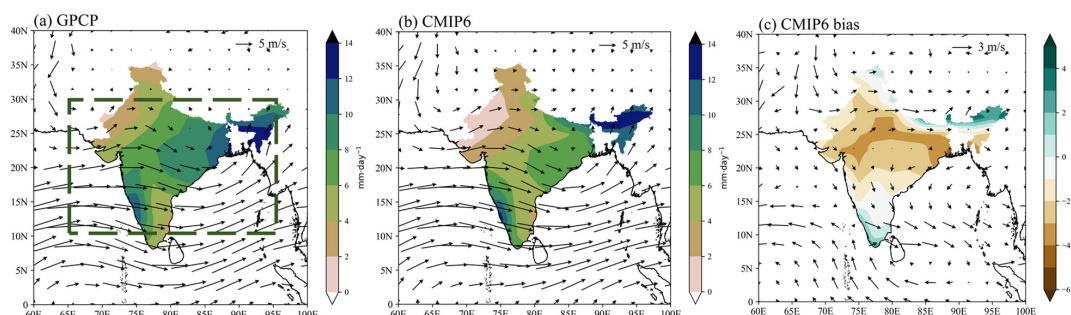
Figure 1. Climatological state distribution of summer monsoon rainfall and 850 hPa wind field in India, 1979–2014. (**a**) GPCP, (**b**) CMIP6 multi-model ensemble, (**c**) model-observation difference (units: mm·d^{-1}); The green box(65~95° E, 10~30° N) indicates the region of Indian summer monsoon rainfall.

Leveraging the Taylor diagram (Figure 2), we conducted an in-depth evaluation of the CMIP6 models' prowess in simulating ISMR climatology. The findings reveal that, for ISMR (Figure 2a), the PCC spanning 35 models and observations fluctuates between 0.6 and 0.9, with a notable 16 models boasting a correlation coefficient above 0.80. The SDR, delineating the simulation from the observation, oscillates between 0.85 and 1.39, and with an RMSE under 0.75, it's evident that the lion's share of CMIP6 models excel in simulating ISMR climatology. Furthermore, the aggregated results from the multi-model ensemble (MME) significantly outpace those of individual models.
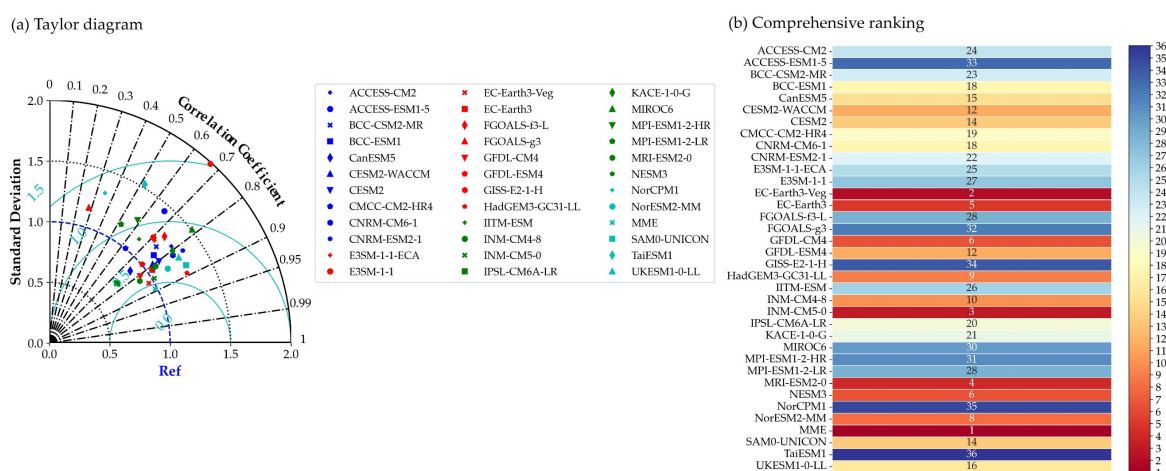

Figure 2. In CMIP6, (**a**) the Taylor diagram illustrating the climatological distribution of ISMR from 1979–2014 as simulated by 35 models relative to observations, and (**b**) the comprehensive ranking of models based on the composite rating indicator M_R; the number on the colors block indicates the model's ranking in terms of its ability to simulate the ISMR composite, with warmer colors indicating a higher ranking.

To furnish a lucid portrayal of the simulation proficiencies of the 35 models under CMIP6's umbrella, we rolled out a holistic rating indicator (Figure 2b). This visualization elucidates the comprehensive M_R ranking, spotlighting the simulation acumen of the 35 models and the collective prowess of the MME for ISMR. Notably, some models, such as EC-Earth3, EC-Earth3-Veg, INM_CM5-0, and MRI-ESM2-0, stand out, showcasing exemplary simulation performance for ISMR climatology. Moreover, the MME's simulation finesse towers over the majority of individual model outcomes.

3.1.2. Evaluation for Interannual Variability

The capability to simulate rainfall over time is a significant measure of a model's performance. The Interannual Variability Score (IVS) and Root Mean Square Error (RMSE) are used to quantify the consistency of interannual variations between model variables and observed variables. Figure 3a displays the IVS for ISMR and ISM, showing that CMIP6 simulations for AIRI and IMI tend to align, with a correlation coefficient R nearing 0.7. The simulated IVS values show a wide range of variations, from 0 to 7.0, indicating that different CMIP6 models have significant discrepancies in simulating the interannual variability of the precipitation index and monsoon index. Figure 3b presents the RMSE for ISMR and ISM. Most models effectively simulate the precipitation intensity of ISMR during historical periods, with generally smaller RMSE values for summer monsoon rainfall. Specifically, CMCC-CM2-HR4, NESM3, and MPI-ESM1-2-LR stand out in simulating the interannual variations of ISMR, with their IVS and RMSE scores surpassing other models. However, these three models do not perform the best in climatology simulations (as seen in Figure 2b). Notably, MPI-ESM1-2-LR has a relatively low performance in climatology simulation, suggesting that the performance of various models in simulating climatology and interannual variations does not necessarily correlate.
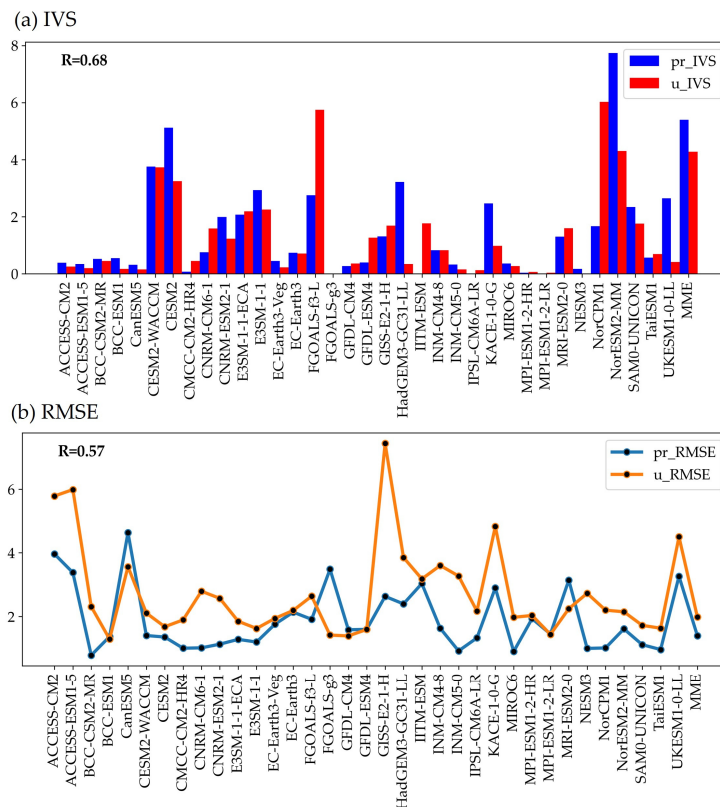

Figure 3. (**a**) IVS and (**b**) RMSE corresponding to the interannual variability in ISMR and the ISM simulated by the CMIP6 model; The closer the IVS and RMSE values are to 0, the better the simulation performance of the model is. R represents the correlation between the inter-annual variation of the ISMR and the ISM (passes 95% confidence test).

3.1.3. Evaluation for Overall Competence

To holistically evaluate the models' prowess in simulating both climatology and inter-annual fluctuations [9], we amalgamated the M_R scores derived from the Taylor diagram with the IVS and RMSE metrics, culminating in a scatter plot that encapsulates the overarching competence of each model (Figure 4). The nexus between the CMIP6 models' aptitude in simulating ISMR, spanning climatology and interannual variability, remains tenuous, evidenced by a modest correlation coefficient of −0.15. The models' distribution appear somewhat diffuse. Predominantly, models either shine in climatological representation or in capturing interannual nuances, seldom both. A select few models emerge as paragons of comprehensive simulation, as spotlighted in the upper right quadrant of Figure 4a. Pertaining to the pivotal ISM indicator, which gauges the model's fidelity in replicating ISMR, its integrated performance appraisal is depicted in Figure 4b. The symbiotic relationship between the models' dexterity in capturing the ISM's temporal (climatology) and spatial (interannual variability) dynamics is similarly tepid, with a correlation coefficient registering at 0.17. Focusing solely on climatological disparities (*x*-axis), certain standout models, such as CESM2-WACCM, EC-Earth3, MRI-ESM2-0, and NorESM2-MM, exhibit exemplary proficiency in both wind field and precipitation climatology.
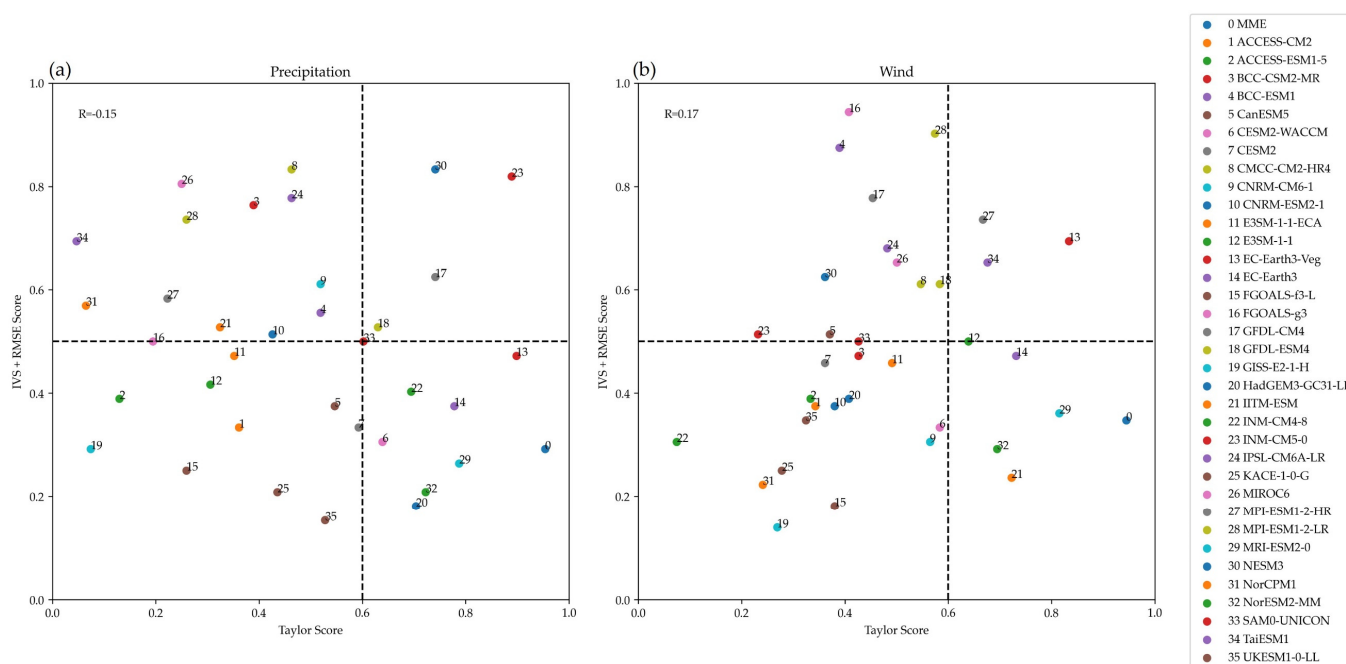
Figure 4. (**a**) ISMR; (**b**) ISM. Scatterplot of patterns based on the Taylor composite score (*x*-axis; climate state) and the interannual variability composite score (*y*-axis; interannual variability); each point represents a pattern, identified by a number on the right. Patterns in the upper right quadrant of the plot represent composite high performance.

Drawing insights from Figure 4, we can distill models that are adept at mirroring both the temporal and spatial intricacies of ISMR, including BCC-ESM1, EC-Earth3-Veg, GFDL-CM4, INM-CM5-0, and SAM0-UNICON. Their cumulative performance—marked by a score exceeding 0.6 on the Taylor diagram coupled with an interannual variability score surpassing 0.5—vaults them into the top echelon among all contenders. In stark contrast, certain models, namely ACCESS-ESM1-5, FGOALS-f3-L, FGOALS-g3, GISS-E2-1-H, and NorCPM1, languish at the opposite end of the performance spectrum.

3.2. Exploring Potential Causes for Biases in ISMR Simulations by CMIP6 Models

Based on the previous research, we selected the best-performing models (pMME) and nonperforming models (nMME) to form model ensembles. We conducted a comparative

analysis of their differences in simulating the ISMR climatology and delved into the potential reasons for the simulation biases. This will enhance our understanding of CMIP6 simulations in the Indian region.

3.2.1. Discrepancies between Prime and Nonperforming Models

To elucidate the disparities between the prime and nonperforming models, the bias maps derived from the multi-model ensemble simulation for ISMR is illustrated in Figure 5. The figure reveals that, in contrast to MME (as seen in Figure 5a), the easterly bias projected by pMME over the northern Bay of Bengal and the Indian Ocean is diminished (as depicted in Figure 5b). Furthermore, there is a marked reduction in the dry bias across central and eastern India, aligning the overall rainfall intensity more closely with the observed data. Unfortunately, the pronounced wet bias over the Indian Ocean and the Western Ghats, as simulated by MME, did not witness substantial improvements within the pMME framework. In the context of nMME (Figure 5c), there is an amplification of the easterly bias stretching from the northern Bay of Bengal to the Arabian Sea. Concurrently, the dry bias in central India is exacerbated, accompanied by an uptick in the wet bias in the southern regions. Collectively, these patterns underscore nMME's subpar simulation prowess concerning the ISM, culminating in pronounced ISMR bias shifts. To encapsulate, pMME's rendition of IMSR climatology stands out in precision, boasting a PCC that surpasses 0.85, and its RMSE markedly undercuts that of nMME (0.55 versus 1.30). Conversely, nMME's portrayal of the Indian summer monsoon is somewhat lackluster, translating to a net decrement in India's rainfall.
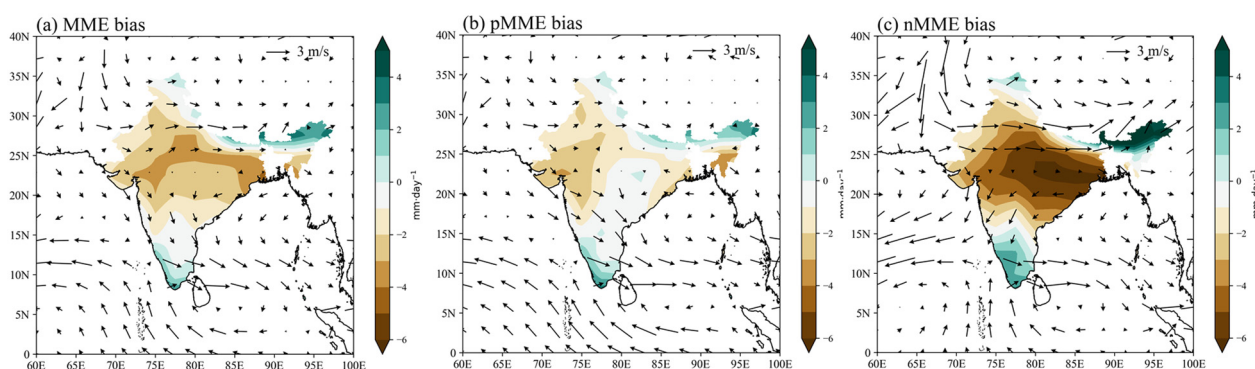

Figure 5. Deviation distribution of CMIP6-simulated Indian summer monsoon rainfall climatology and 850 hPa wind climatology: (**a**) MME, (**b**) pMME, and (**c**) nMME.

3.2.2. Investigating the Role of Sea Surface Temperature Anomalies in Modulating the ISMR

The variation in the Sea Surface Temperature (SST) of the Indian Ocean acts as a pivotal driver for the ISM [5,11,17]. It influences the strength of the low-level southwest winds, subsequently modulating the volume of the Indian summer monsoon rainfall. Compared to CMIP, AMIP models, without considering the impact of SST, can simulate the intensity of an ISM with relative accuracy. This further suggests that the SST variations in the various climate models of CMIP6 can introduce biases in the simulation of ISMR.

The Northern Indian Ocean (NIO) exhibits a cold bias, especially during the spring (MAM, Figure 6a). This results in a weakened meridional land–sea thermal contrast, with the cold bias gradually diminishing from spring to autumn. The cold-biased SST suppresses local convection and latent heat release in the NIO, subsequently weakening the meridional temperature gradient. This leads to a diminished summer monsoon, thereby affecting the formation and distribution of ISMR [5,6]. To validate the physical processes behind the cold SST bias leading to a weakened monsoon and consequently impacting ISMR, we analyzed the relationship between precipitation biases simulated by the majority of CMIP6 models (including pMME, nMME, and MME) and related physical factors (Figure 6). The results

indicate a consistent presence across numerous CMIP6 models of the physical process where the cold SST bias in the spring NIO leads to reduced ISMR. Most models reveal a significant positive correlation between the SST bias in spring NIO and the summer (JJAS) SST bias (Figure 6a), with R = 0.65 (at the 99% confidence level). Additionally, significant positive correlations (at the 95% confidence level) are evident between the spring SST bias and both ISM bias (Figure 6b) and ISMR bias (Figure 6c). This implies that the cold SST bias in the spring NIO significantly impacts the strength of the summer monsoon, subsequently affecting the model's simulation of ISMR. Notably, the cold SST bias simulated by most prime models, including the Prime Model Mean Ensemble (pMME), is more moderate (Figure 6a). The average cold SST bias improves from −1.66 K in the Nonperforming Model Mean Ensemble (nMME) to −1.02 K in the pMME. This enables the pMME to more accurately simulate the land–sea thermal contrast and monsoon circulation characteristics, thereby enhancing the simulation accuracy of ISMR.
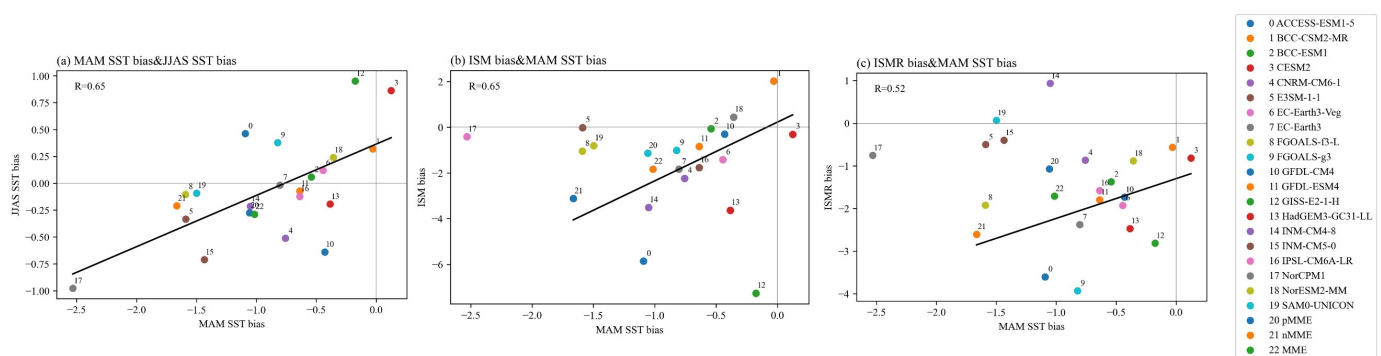
Figure 6. Relationship between precipitation bias and associated physical factors simulated by CMIP6 (including excellent and poor models and multi-model ensembles): (**a**) MAM SST vs. JJAS SST for NIO; (**b**) MAM SST vs. ISM; (**c**) MAM SST vs. ISMR. Each point represents a mode (including pMME and nMME as well as MME), identified by a number on the right side; the correlation coefficient between the two is indicated by R in the upper left corner of the Figure (all passing the 95% confidence level).

In conclusion, the SST of the NIO during spring and summer is significantly correlated and play a crucial role in monsoon rainfall development. Therefore, the cold SST bias in the NIO is a key factor affecting the accuracy of ISMR simulations in CMIP6.

3.2.3. Assessing the Contributions of Atmospheric Circulation Dynamics to ISMR Variability

The atmospheric circulation serves as a vital backdrop for ISMR. The three model groups essentially capture the characteristics of the Indian summer monsoon circulation (Figure 7). Compared to ERA5 (Figure 7a), the pMME simulation (Figure 7c) shows a strengthened thermal low over the South Asian continent and an intensified subtropical high in the Southern Hemisphere. The enhanced meridional pressure gradient results in stronger low-level southwesterly winds in the southern region of India, facilitating moisture transport. In contrast, nMME (Figure 7d) fails to simulate the positive pressure bias in the Southern Hemisphere, which is unfavorable for moisture transport across the Indian Ocean. Quantitatively (Figure 7i), the meridional pressure gradient simulated by pMME is stronger than that of ERA5 (Figure 7a). The easterly bias in the lower atmosphere over southern India, as depicted in Figure 7b–d, suppresses moisture transport. Additionally, the cyclonic circulation anomaly in northeastern India, as simulated by nMME, further weakens the southwesterly flow over India. In quantitative terms, the IMI simulated by nMME deviates more from the observed values. As shown in Figure 7f–h, the strength of the West Pacific subtropical high is beneficial for the development and maintenance of ISMR. The southeasterly winds on the western side of the subtropical high transport moisture

to central and eastern India. However, compared to pMME, nMME underestimates the strength of the subtropical high, with its position shifted northward, leading to reduced rainfall in northern India. Furthermore, all three model ensembles exhibit a negative bias in the 300 hPa meridional wind in the troposphere, which also results in a weaker simulation intensity for ISMR.
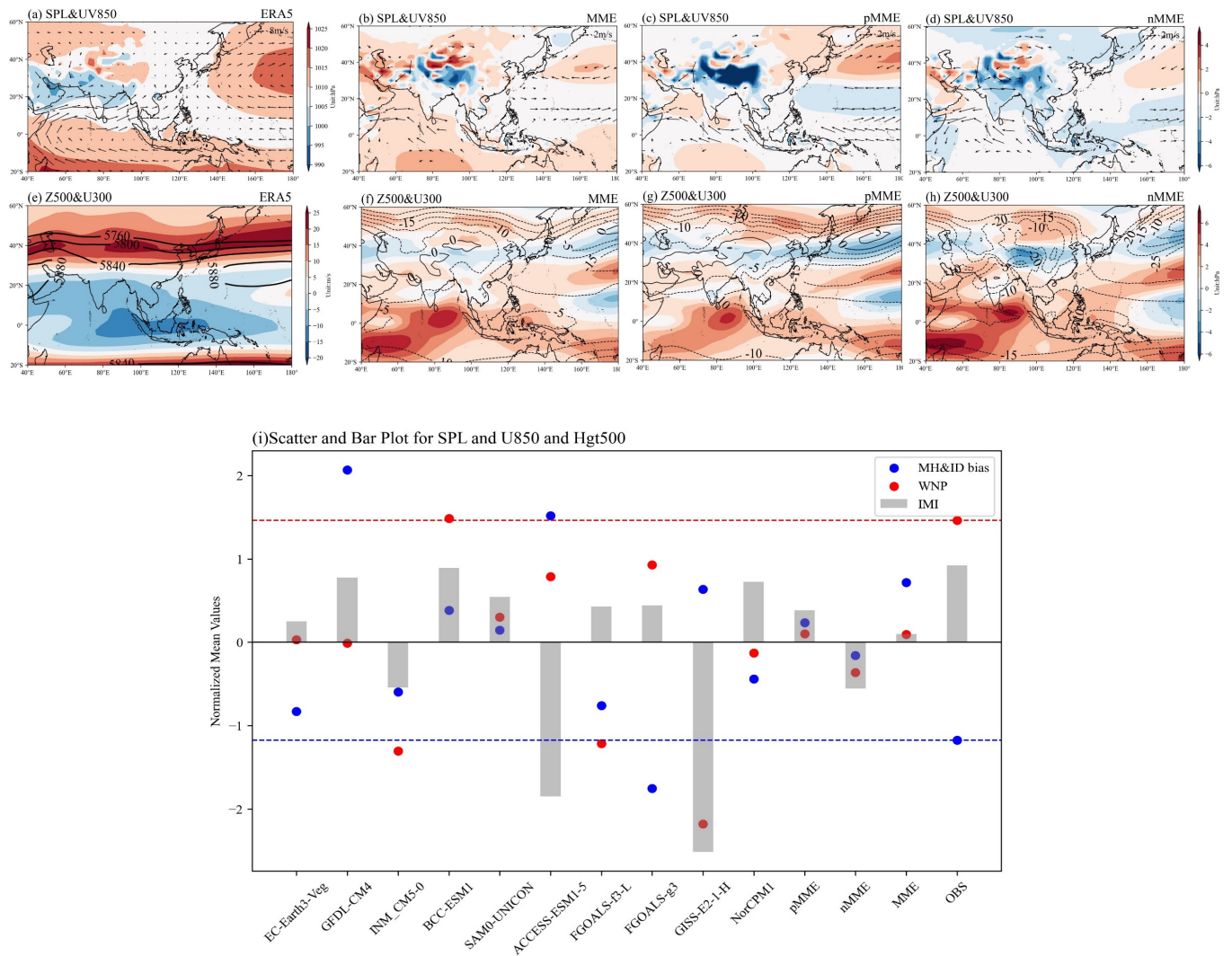

Figure 7. (**a**) Summer sea-level pressure field (shaded, unit: hPa) and 850 hPa wind field (vector arrows, unit: m/s) from ERA5 for the period 1979–2014; (**b**) Simulation bias between MME and ERA5; (**c**) Bias in pMME; (**d**) Bias in nMME; (**e**) Summer 500 hPa geopotential height field (contour lines, unit: hPa) and 300 hPa zonal wind field (shaded, unit: m/s) from ERA5 for the period 1979–2014; (**f**) Simulation bias between MME and ERA5; (**g**) Bias in pMME; (**h**) Bias in nMME; (**i**) CMIP6-simulated standardized atmospheric circulation index. The blue dots represent the deviation of the Mascarene high pressure from the Asian low pressure on the sea level pressure field; the red dots represent the Northwest Pacific high pressure index on the 500 hPa geopotential height field; and the grey bars represent the Indian summer wind index on the 850 hPa wind field. The dotted lines indicate the magnitude of the observations.

In summary, the atmospheric circulation of the Indian summer monsoon is pivotal for monsoon rainfall. The minor biases in the simulation of various atmospheric circulation elements by pMME play a significant role in the accurate simulation of the ISMR climatology.

3.3. Anticipated Shifts in ISMR: Insights from CMIP6 Projections

Leveraging the adept representation of ISMR's climatology by CMIP6 models, it becomes imperative to delve into their predictive efficacy for impending shifts. From the suite of 35 models, 22 were cherry-picked, each encompassing data spanning 3 prospective emission trajectories: SSP1-2.6, SSP2-4.5, and SSP5-8.5. Temporal demarcations for the 21st century are delineated as follows: the near-term spans 2021–2040, mid-century encapsulates 2041–2060, and the terminal phase stretches from 2081 to 2100.

Figure 8 elucidates the ISMR prognostications for the ensuing century as inferred from the CMIP6 multi-model ensemble. Across the board of projected emission scenarios, an ascendant trajectory in precipitation indices is discernible among the model ensembles. Up to the 2040 threshold, the augmentation patterns across the triad of scenarios are congruent. However, after this juncture, while the inclines in SSP1-2.6 and SSP2-4.5 taper off, the SSP5-8.5 trajectory manifests a relentless surge, approximating a 35% increment. In contrast to the MME, the pMME's projections intimate a more subdued precipitation augmentation across the SSP spectrum, whereas the nMME's projections are more pronounced. On the spatial front (figure omitted), the ensemble consensus is a more accentuated precipitation uptick in the northern over the southern quadrants of India, and the western regions compared to their eastern counterparts. Notably, the nMME's ISMR projections are the most salient, trailed by the MME, and, subsequently, the pMME. Benchmarked against the historical reference period, CMIP6 models prognosticate that by the twilight of the 21st century, under the aegis of the SSP2-4.5 scenario, precipitation will burgeon by 8–18%, while under the SSP5-8.5 scenario, the surge could range between 23–44%.
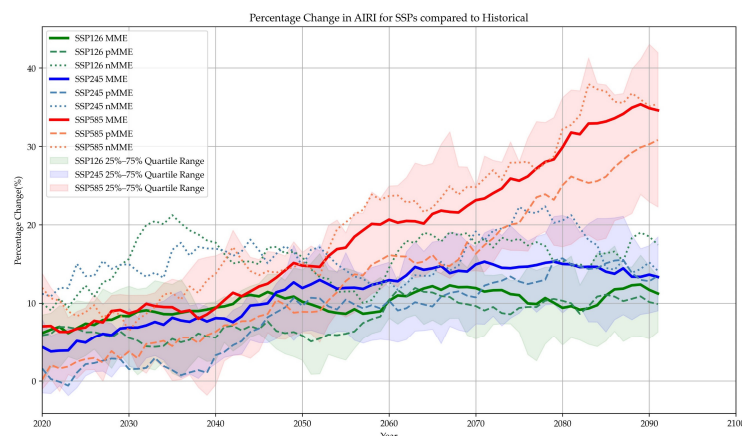
Figure 8. CMIP6 modelling of time series of ISMR changes (units: %) under future emission scenarios SSP1-2.6 (green), SSP2-4.5 (blue), and SSP5-8.5 (red) (relative to historical base period 1979–2014). Solid, dashed, and dotted lines indicate the simulation results for MME, pMME, and nMME, respectively. Shaded areas show the 25th to 75th percentile distributions of the modes to characterize the inter-model uncertainty. The time series are smoothed with a 9a running mean filter.

4. Discussion

The proficiency demonstrated by a significant cohort of CMIP6 models in capturing the climatological complexities of the Indian Summer Monsoon Rainfall (ISMR) marks a notable progression in climate modeling. However, these models exhibit a tendency to overestimate precipitation intensity over the Western Ghats while concurrently underestimating it in the central and eastern regions of India. This pattern echoes the findings of previous research, underscoring a recurrent obstacle in achieving accurate regional precipitation simulations [25,26]. The discrepancy in representing interannual variability when compared to empirical observations underscores the critical need for model enhancement. This requirement aligns with the hypothesis that a detailed understanding of regional climatic mechanisms is essential for improving simulation fidelity [27,28].

Moreover, the demarcation of proficient models, such as BCC-ESM1, EC-Earth3-Veg, GFDL-CM4, INM-CM5-0, and SAM0-UNICON, in their ability to capture the spatiotemporal variations in ISMR, suggests the potential benefits of a multi-model ensemble approach. This concept is in harmony with the broader scientific consensus advocating for a weighted ensemble approach to enhance the precision of future climate projections [29,30]. The recognition of the Northern Indian Ocean's spring sea surface temperature cold bias as a cardinal determinant influencing ISMR simulation precision dovetails with the overarching comprehension of ocean–atmosphere interactions in orchestrating monsoonal dynamics [31].

Projected augmentation in ISMR as we verge towards the twilight of the 21st century across all emission scenarios, with a conspicuous surge under the SSP5-8.5 scenario, unfolds as a salient revelation. The spatial heterogeneity in precipitation augmentation across disparate regions of India underscores the regional disparities in climate change ramifications, a theme that echoes the broader climate change discourse. The nMME's projection of a more pronounced percentage escalation for ISMR amplifies the implications of model selection and emission scenarios on ISMR's future trajectories, offering critical insights for the formulation of climate-centric policies.

Moreover, the findings herald promising directions for future research, encompassing a deeper exploration into the underlying mechanisms contributing to simulation biases, probing the potential of higher-resolution models and regional climate downscaling studies in enhancing ISMR simulation accuracy, and assessing the repercussions of varying emission scenarios on ISMR's future trajectories. The quest to rectify the identified biases, particularly in portraying physical processes in mountainous regions, remains a crucial frontier for advancing the global climate modeling domain. This study significantly augments the broader endeavor of refining climate models to better inform climate-centric policy frameworks and adaptation strategies in a region where monsoonal dynamics are a linchpin for socio-economic sustenance.

5. Conclusions

This study evaluates the simulation performance of 35 CMIP6 models in terms of the climatology and interannual variability of ISMR. Based on comprehensive simulation capabilities, the models were ranked, and prime and nonperforming model ensembles were identified for analysis alongside the MME. The research primarily contrasts the differences between pMME and nMME in historical simulations and future projections, delving into the key factors influencing simulation biases. The main conclusions are summarized as follows:

(1) A significant portion of the CMIP6 models adeptly encapsulate the climatological nuances of ISMR. However, there is a propensity to overemphasize the precipitation intensity over the Western Ghats while underrepresenting it in India's central and eastern regions. The interannual variability simulated by these models exhibits a marked divergence from actual observations. While certain models shine in either climatology or interannual variability, a tangible correlation between these two performance metrics remains elusive. After a comprehensive assessment, models that best capture the spatiotemporal variations of ISMR include BCC-ESM1, EC-Earth3-Veg, GFDL-CM4, INM-CM5-0, and SAM0-UNICON.

(2) The pMME's prowess in simulating ISMR's climatology is distinctly superior to that of both the MME and nMME. This is particularly evident in the portrayal of the southwest monsoon's vigor and the precipitation patterns over central and eastern India. An in-depth analysis ascertains that the Northern Indian Ocean's (NIO) spring SST cold bias is a cardinal element affecting the precision of ISMR simulations. The enhanced acumen of pMME in simulating diverse atmospheric circulation facets is instrumental in the accurate depiction of ISMR's climatology.

(3) As we approach the twilight of the 21st century, projections indicate an uptick in ISMR across all three emission trajectories, with the surge under the SSP5-8.5 scenario being markedly more accentuated than its SSP1-2.6 and SSP2-4.5 counterparts. All

three model ensembles anticipate a more pronounced percentage augmentation in precipitation in northern India relative to the southern regions, and a more substantial increase in the west than the east. Intriguingly, the nMME's projected percentage escalation for ISMR considerably outstrips the projections of both MME and pMME. These revelations underscore the profound ramifications of varying emission scenarios on ISMR's future trajectories, furnishing invaluable insights for the formulation of climate-centric policies.

References

1. Saha, K.R.; Mooley, D.A.; Saha, S. The Indian monsoon and its economic impact. *Geojournal* **1979**, *3*, 171–178. [CrossRef]
2. Gusain, A.; Ghosh, S.; Karmakar, S. Added value of CMIP6 over CMIP5 models in simulating Indian summer monsoon rainfall. *Atmos. Res.* **2019**, *232*, 104680. [CrossRef]
3. Jiang, W.H.; Chen, H.P. Simulation and projection of extreme temperature changes in the mid-high latitudes of Asia by CMIP6 models. *Trans. Atmos. Sci.* **2021**, *44*, 592–603. (In Chinese)
4. Song, Y.J.; Li, X.F.; Bao, Y.; Song, Z.; Wei, M.; Shu, Q.; Yang, X. FIO-ESM v2.0 Outputs for the CMIP6 Global Monsoons Model Intercomparison Project Experiments. *Adv. Atmos. Sci.* **2020**, *37*, 1045–1056. [CrossRef]
5. Wang, Z.Q.; Li, G.; Yang, S. Origin of Indian summer monsoon rainfall biases in CMIP5 multimodel ensemble. *Clim. Dyn.* **2018**, *51*, 755–768. [CrossRef]
6. Sperber, K.R.; Annamalai, H.; Kang, I.S.; Kitoh, A.; Moise, A.; Turner, A.; Wang, B.; Zhou, T. The Asian summer monsoon: An intercomparison of CMIP5 vs. CMIP3 simulations of the late 20th century. *Clim. Dyn.* **2013**, *41*, 2711–2744. [CrossRef]
7. Boos, W.R.; Hurley, J.V. Thermodynamic bias in the multimodel mean boreal summer monsoon. *J. Clim.* **2013**, *26*, 2279–2287. [CrossRef]
8. Levine, R.C.; Turner, A.G.; Marathayil, D.; Martin, G.M. The role of northern Arabian Sea surface temperature biases in CMIP5 model simulations and future projections of Indian summer monsoon rainfall. *Clim. Dyn.* **2013**, *41*, 155–172. [CrossRef]
9. Jiang, Z.H.; Li, W.; Xu, J.J.; Li, L. Extreme Precipitation Indices over China in CMIP5 Models. Part I: Model Evaluation. *J. Clim.* **2015**, *28*, 8603–8619. [CrossRef]
10. Srerkala, P.P.; Babu, C.A.; Rao, V.B. On the simulation of northeast monsoon rainfall over southern peninsular India in CMIP5 and CMIP6 models. *Theor. Appl. Climatol.* **2022**, *150*, 969–986. [CrossRef]

11. Guo, P.W.; Shen, C.; Dong, L.N.; Zhang, P.Q.; Yin, L.W. Observational analysis and simulation assessment of sea-land thermal changes in the Asian monsoon region. *Trans. Atmos. Sci.* **2017**, *40*, 215–223. (In Chinese)

12. Turner, A.G.; Annamalai, H. Climate change and the South Asian summer monsoon. *Nat. Clim. Chang.* **2012**, *2*, 587–595. [CrossRef]

13. Woo, S.; Singh, G.P.; Oh, J.H.; Lee, K.-M. Projection of seasonal summer precipitation over Indian sub-continent with a high-resolution AGCM based on the RCP scenarios. *Meteorol. Atmos. Phys.* **2019**, *131*, 897–916. [CrossRef]

14. Jayasankar, C.B.; Surendran, S.; Rajendran, K. Robust signals of future projections of Indian summer monsoon rainfall by IPCC AR5 climate models: Role of seasonal cycle and interannual variability. *Geophys. Res. Lett.* **2015**, *42*, 3513–3520. [CrossRef]

15. Si, S.; Bi, X.Q.; Kong, X.H.; Hua, W. Analysis of the spatiotemporal distribution characteristics of major greenhouse gases and aerosol emissions intensity in CMIP6 scenarios. *Clim. Environ. Res.* **2020**, *25*, 366–384. (In Chinese)

16. Eyring, V.; Bony, S.; Meehl, G.A.; Senior, C.A.; Stevens, B.; Stouffer, R.J.; Taylor, K.E. Overview of the Coupled Model Intercomparison Project Phase 6 (CMIP6) experimental design and organization. *Geosci. Model Dev.* **2016**, *9*, 1937–1958. [CrossRef]

17. He, L.Q.; Zhou, T.J.; Chen, X.L. South Asian summer rainfall from CMIP3 to CMIP6 models: Biases and improvements. *Clim. Dyn.* **2022**, *61*, 1049–1061. [CrossRef]

18. Ha, K.J.; Moon, S.; Timmermann, A.; Kim, D. Future changes of summer monsoon characteristics and evaporative demand over Asia in CMIP6 simulations. *Geophys. Res. Lett.* **2020**, *47*, e2020GL087492. [CrossRef]

19. Almazroui, M.; Saeed, S.; Saee, F.; Islam, M.N.; Ismail, M. Projections of Precipitation and Temperature over the South Asian Countries in CMIP6. *Earth Syst. Environ.* **2020**, *4*, 297–320. [CrossRef]

20. Liu, J.; Wang, B.; Kuang, X.; Soon, W.; Zorita, E. Centennial variations of the global monsoon precipitation in the last millennium: Results from ECHO-G model. *J. Clim.* **2009**, *22*, 2356–2371. [CrossRef]

21. Li, R.Q.; Lü, S.H.; Han, B. Simulation of the Austral-Asian monsoon circulation and its variability by 10 CMIP5 models. *J. Trop. Meteorol.* **2013**, *29*, 749–758. (In Chinese)

22. Taylor, K.E. Summarizing multiple aspects of model performance in a single diagram. *J. Geophys. Res. Atmos.* **2001**, *106*, 7183–7192. [CrossRef]

23. Schuenemann, K.C.; Cassano, J.J. Changes in synoptic weather patterns and Greenland precipitation in the 20th and 21st centuries: 2. Analysis of 21st century atmospheric changes using self-organizing maps. *Clim. Dyn.* **2010**, *115*, D05108. [CrossRef]

24. Chen, W.L.; Jiang, Z.; Li, L. Probabilistic projections of climate change over China under the SRES A1B scenario using 28 AOGCMs. *J. Clim.* **2011**, *24*, 4741–4756. [CrossRef]

25. Liu, Z.; Bollasina, M.A.; Wilcox, L.J.; Rodríguez, J.M.; Regayre, L.A. Contrasting the role of regional and remote circulation in driving Asian monsoon biases in MetUM GA7.1. *J. Geophys. Res. Atmos.* **2021**, *126*, e2020JD034342. [CrossRef]

26. Hanf, F.S.; Annamalai, H. Systematic errors in South Asian monsoon precipitation: Process-based diagnostics and sensitivity to entrainment in NCAR models. *J. Clim.* **2020**, *33*, 2817–2840. [CrossRef]

27. Choudhury, B.A.; Rajesh, P.V.; Zahan, Y.; Goswami, B.N. Evolution of the Indian summer monsoon rainfall simulations from CMIP3 to CMIP6 models. *Clim. Dyn.* **2022**, *58*, 2637–2662. [CrossRef]

28. Mahendra, N.; Chowdary, J.S.; Darshana, P.; Sunitha, P.; Parekh, A.; Gnanaseelan, C. Interdecadal modulation of interannual ENSO-Indian summer monsoon rainfall teleconnections in observations and CMIP6 models: Regional patterns. *Int. J. Climatol.* **2021**, *41*, 2528–2552. [CrossRef]

29. Yu, T.; Chen, W.; Gong, H.; Feng, J.; Chen, S. Comparisons between CMIP5 and CMIP6 models in simulations of the climatology and interannual variability of the east Asian summer Monsoon. *Clim. Dyn.* **2023**, *60*, 2183–2198. [CrossRef]

30. Rajendran, K.; Surendran, S.; Varghese, S.J.; Sathyanath, A. Simulation of Indian summer monsoon rainfall, interannual variability and teleconnections: Evaluation of CMIP6 models. *Clim. Dyn.* **2022**, *58*, 2693–2723. [CrossRef]

31. Chowdary, J.S.; Bandgar, A.B.; Gnanaseelan, C.; Luo, J.-J. Role of tropical Indian Ocean air–sea interactions in modulating Indian summer monsoon in a coupled model. *Atmos. Sci. Lett.* **2015**, *16*, 170–176. [CrossRef]